Excitable dynamics and threshold sets in nonlinear systems

Michal Voslař and Igor Schreiber*
Department of Chemical Engineering and Center for Nonlinear Dynamics of Chemical and Biological Systems, Prague Institute of Chemical Technology, Technická 5, 166 28 Prague 6, Czech Republic
(Received 15 July 2003; published 27 February 2004)

Following our previous work [J. Zagora *et al.*, Faraday Discuss. **120**, 313 (2001)], we present a quantitative definition of a threshold that separates large-amplitude excitatory responses and small-amplitude nonexcitatory responses to a perturbation of an excitable system with a single globally attracting steady state. For systems with two variables, finding the threshold set is formulated as a boundary value problem supplemented by a condition of a maximum separation rate. For this highly nonlinear problem we formulate a numerical method based on the use of multiple shooting and continuation methods. The threshold phenomena are examined by using an example dynamical system with chemical reaction—the bromate-sulfite-ferrocyanide system. In a model of this reaction we find the threshold set, construct a bifurcation diagram and discuss how excitability can vanish. These results are compared with recent experiments. We also discuss relevance of other definitions of the excitability threshold including the concept of nullclines.

DOI: 10.1103/PhysRevE.69.026210 PACS number(s): 05.45.−a, 82.20.−w, 82.20.Wt

I. INTRODUCTION

Excitability represents one of the basic mechanisms utilized in living organisms [1,2], because it allows to react adequately to external stimuli, examples are biochemistry of sensory perception [2], neural and muscular activity [3–5], metabolic regulation [6], etc. Excitability also frequently occurs in chemical, biochemical, and physical systems [7–10]. In essence, it is an ability to amplify a superthreshold pulse; the existence of the threshold helps to ensure distinction of sensible information from noise, while the amplification is a necessary condition for an effective response. More technically, when a system operating at a stable steady state is subject to a small-size perturbation, the deviation from the steady state may decrease uniformly. However, some systems significantly amplify perturbations exceeding certain size for a transient period of time before the response amplitude begins to shrink. Systems possessing such transient dynamics are called excitable. Very often, excitability is associated with a spatial transport, for instance, in the form of pulse waves in reaction-diffusion systems. Here we will focus on ''lumped parameter'' systems, which are not spatially extended. If such systems are periodically perturbed, complex firing patterns may result and the analysis of threshold behavior presented here is a prerequisite for understanding these patterns.

Intuitively, excitability is associated with a threshold set which delineates a boundary between perturbations that become amplified and those that are damped. In an excitable system with multiple steady states the threshold set is simply formed by a stable separatrix of a saddle—as the size of the perturbation is increased the transition from a nonexcitatory to an excitatory response is discontinuous [11]. If there is a unique steady state, however, the transition is in fact smooth, albeit very sharp. Yet, on the observational level, there appears a distinct threshold associated in some way with a steepest change in the amplitude of the response. This type of excitability is very frequent in nonlinear systems.

In our previous work [12] a basic quantitative formulation of the threshold set in the presence of a unique steady state was introduced. In Secs. II and III we give a detailed account and extend this concept by describing an iterative procedure for numerically accurate location of the threshold. This allows us to understand how excitability vanishes and how it is interlinked with bistability and periodic oscillations. In Sec. IV we provide an example of an excitable chemical reaction, calculate the threshold set and then construct and discuss a corresponding bifurcation diagram. Comparison with other approaches is discussed in Secs. IV and V.

II. THEORY

We assume that a dynamical system is given in terms of ordinary differential equations

$$\frac{d\boldsymbol{x}}{dt}=\boldsymbol{v}(\boldsymbol{x}), \quad \boldsymbol{x}\in R^n. \tag{1}$$

The vector field $\boldsymbol{v}$ is implicitly assumed to depend on external parameters. In general, the threshold set $\mathcal{T}$ should be a smooth codimension one surface having a codimension two end about which trajectories of Eq. (1) corresponding to excitations wind. For this reason we assume $\mathcal{T}$ to be invariant under the flow $\boldsymbol{\varphi}(\boldsymbol{x},t)$ of Eq. (1) in negative time direction, i.e., $\boldsymbol{\varphi}(\mathcal{T},t)\subseteq\mathcal{T}$ for all $t<0$. Therefore the threshold set must be a (negatively directed) semiorbit in a two-variable system, a one-parameter smooth family of semiorbits in a three-variable system, etc. A traditional concept of the threshold being a (repelling) piece of a nullcline manifold [1,5] lacks the invariance property and only in the infinitely fast autocatalytic variable limit the two concepts merge.

For simplicity, we assume that the system has two dynamical variables $n=2$, extension to more than two variables is possible. Let $\boldsymbol{x}_S$ be the steady state point, that is, $\boldsymbol{x}_S$ satisfies the equation

*Electronic address: igor.schreiber@vscht.cz

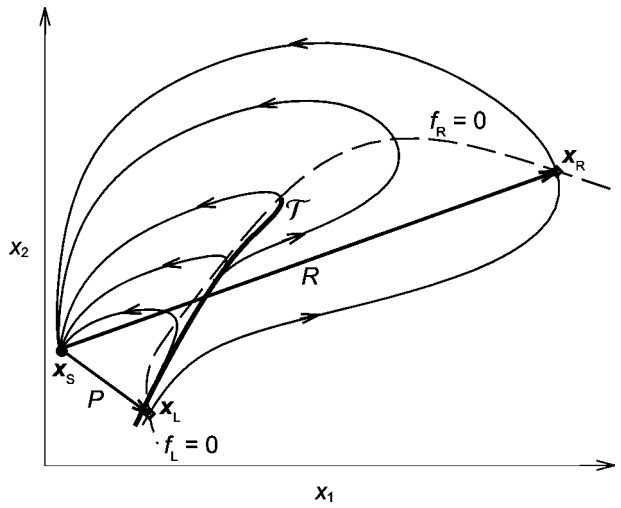

FIG. 1. Schematic phase portrait showing a general segment of an excitatory orbit from a point $\boldsymbol{x}_L$ to $\boldsymbol{x}_R$ satisfying boundary conditions (3) and (5), respectively (dashed line), the perturbation P, the response R, and the threshold set $\mathcal{T}$ (thick line).

$$\boldsymbol{v}(\boldsymbol{x}) = \boldsymbol{0}. \tag{2}$$

To locate the threshold, we formulate a boundary value problem for a finite segment of the threshold orbit beginning at a point $\boldsymbol{x}_L$ and terminating at another point $\boldsymbol{x}_R$, for schematic representation see Fig. 1. The point $\boldsymbol{x}_L$ is specified by applying a perturbation shifting the initial rest state $\boldsymbol{x}_S$ to $\boldsymbol{x}_L$ so that

$$f_L = \boldsymbol{v}_L \cdot (\boldsymbol{x}_L - \boldsymbol{x}_S) = \sum_{i=1}^{n} [v_{Li}(x_{Li} - x_{Si})] = 0. \tag{3}$$

By virtue of Eq. (3), the orbit passing through x_L is locally at a minimum distance P from the steady state which we take as the size (or amplitude) of the pulse

$$P = \|\boldsymbol{x}_L - \boldsymbol{x}_S\| = \sqrt{\sum_{i=1}^{n} (x_{Li} - x_{Si})^2}. \tag{4}$$

Thus P is a minimal perturbation amplitude for the given orbit. The system (1) responds to the perturbation by a motion along the orbit based at $\boldsymbol{x}_L$, the perturbation becomes amplified, eventually reaching a point $\boldsymbol{x}_R$ such that

$$f_R = \boldsymbol{v}_R \cdot (\boldsymbol{x}_R - \boldsymbol{x}_S) = 0. \tag{5}$$

The response amplitude R,

$$R = \|\boldsymbol{x}_R - \boldsymbol{x}_S\|, \tag{6}$$

at that point is, by virtue of Eq. (5), at its maximum. Equations (3) and (5) are formally equivalent and each of them defines a part of the same curve in the state space of Eq. (1), see Fig. 1; the two parts meet at a point where P and R become equal.

Let us define a relative amplification as the increase in amplitude from $\boldsymbol{x}_L$ to $\boldsymbol{x}_R$ relative to the amplitude of perturbation

$$r = \frac{R - P}{P}. \tag{7}$$

All orbit segments satisfying boundary conditions (3) and (5) form a smooth family which can be parametrized by P, and consequently r can be viewed as a function of P. It can be shown that the first derivative of this function is given by

$$\frac{dr}{dP} = \frac{\mathrm{grad}\, r \cdot \boldsymbol{d}^0}{\mathrm{grad}\, P \cdot \boldsymbol{d}^0}, \tag{8}$$

where $\mathrm{grad} = d/d\boldsymbol{x}_L$, and $\boldsymbol{d}^0$ is a normalized vector tangent to the curve defined by Eq. (3) at $\boldsymbol{x}_L$:

$$\boldsymbol{d}^0 \cdot \frac{df_L}{d\boldsymbol{x}_L} = 0, \quad \|\boldsymbol{d}^0\| = 1. \tag{9}$$

The derivative in Eq. (8) plays a role of a sensitivity coefficient characterizing variations of the response with respect to perturbation amplitude, and allows for a definition of the threshold because r is expected to grow most significantly with P just on the orbit segment lying on the threshold set $\mathcal{T}$. We call this sensitivity coefficient a *separation rate* and use it to single out a particular orbit segment connecting $\boldsymbol{x}_L$ and $\boldsymbol{x}_R$ so that dr/dP is at maximum

$$\frac{dr}{dP} \overset{!}{=} \max. \tag{10}$$

The *threshold set* $\mathcal{T}$ is then defined as the semiorbit passing through $\boldsymbol{x}_L$ and terminating at $\boldsymbol{x}_R$ which extends to arbitrary negative times. The constraint (10) is complemented by a condition for an orbit with the smallest possible dr/dP. The associated orbit, in a sense, represents a typical excitatory response and therefore we refer to it as a *characteristic excitation*. Note that an orbit with a maximal relative amplification r corresponding to the point of zero dr/dP is found between the threshold set and the characteristic excitation. Taking into account the commonly accepted qualitative definition of an excitable system as providing (relatively) large-amplitude responses to (relatively) small superthreshold perturbations, it is convenient to add a supplementary constraint to Eq. (10) requiring that the relative amplification for both extreme orbits satisfies

$$r \geqslant 1. \tag{11}$$

This ensures that all the orbits between the threshold set and the characteristic excitation are sufficiently amplifying the perturbation.

Since the Euclidean distance used in defining P and R depends on scaling, we need to assume that the variables in Eq. (1) are given in their natural scale. As a threshold phenomenon, excitability cannot be made scale independent, because the measurement of both the perturbation and response amplitudes involves more than one variables.

III. NUMERICAL METHOD FOR FINDING THRESHOLD SETS

In the following we develop a numerical approach for finding the threshold orbit by employing the shooting method and combining it with the continuation method [13,14]. The formula (8) requires calculation of grad P and grad r. The former is simply expressed as

$$\operatorname{grad} P = \frac{dP}{d\boldsymbol{x}_L} = \frac{\boldsymbol{x}_L - \boldsymbol{x}_S}{P}. \tag{12}$$

The expression for the latter is more subtle. Since the points $\boldsymbol{x}_L$, $\boldsymbol{x}_R$ belong to one orbit, the initial (left) point on the segment is mapped to the terminal (right) point by the flow φ of Eq. (1),

$$\boldsymbol{x}_R = \boldsymbol{\varphi}(\boldsymbol{x}_L, T(\boldsymbol{x}_L)), \tag{13}$$

where the time T of travel between the points depends on $\boldsymbol{x}_L$. By formally differentiating Eq. (7) with respect to $\boldsymbol{x}_L$, we obtain

$$\frac{dr}{d\boldsymbol{x}_L} = \frac{\dfrac{P}{R}\displaystyle\sum_{i=1}^{n}\left[\frac{d\varphi_i(\boldsymbol{x}_L, T(\boldsymbol{x}_L))}{d\boldsymbol{x}_L}(x_{Ri} - x_{Si})\right] - \frac{R}{P}(\boldsymbol{x}_L - \boldsymbol{x}_S)}{\|\boldsymbol{x}_L - \boldsymbol{x}_S\|^2}, \tag{14}$$

where

$$\frac{d\varphi_i(\boldsymbol{x}_L, T(\boldsymbol{x}_L))}{d\boldsymbol{x}_L} = \frac{\partial \varphi_i}{\partial \boldsymbol{x}_L} + \frac{\partial \varphi_i}{\partial T}\frac{dT}{d\boldsymbol{x}_L}. \tag{15}$$

The term $U = \{\partial \varphi_i / \partial x_{Lj}\}$ is the fundamental matrix obtained by integrating first variational equations of the system (1) along the orbit segment. The derivative of the flow with respect to time is just the vector field $\boldsymbol{v}_R$ at $\boldsymbol{x}_R$ and the term $dT/d\boldsymbol{x}_L$ is obtained by differentiating the right boundary condition (5) with respect to $\boldsymbol{x}_L$,

$$\frac{df_R}{d\boldsymbol{x}_L} = \sum_{i=1}^{n}\left[\frac{d\varphi_i(\boldsymbol{x}_L, T(\boldsymbol{x}_L))}{d\boldsymbol{x}_L} v_{Ri} + \frac{dv_{Ri}}{d\boldsymbol{x}_L}(x_{Ri} - x_{Si})\right] = \boldsymbol{0}, \tag{16}$$

where

$$\frac{dv_{Ri}}{d\boldsymbol{x}_L} = \sum_{k=1}^{n}\left[\frac{dv_{Ri}(\boldsymbol{x}_R)}{d\boldsymbol{x}_R}\frac{d\varphi_k(\boldsymbol{x}_L, T(\boldsymbol{x}_L))}{d\boldsymbol{x}_L}\right], \tag{17}$$

and $J_R = \{dv_{Ri}/dx_{Rj}\}$ is the Jacobian of the vector field in Eq. (1) evaluated at $\boldsymbol{x}_R$. The formula (16) and (17) can be rearranged to give an explicit expression for the derivative of T with respect to $\boldsymbol{x}_L$:

$$\frac{\partial T}{\partial \boldsymbol{x}_{Lj}} = -\frac{\displaystyle\sum_{i=1}^{n}\left[(x_{Ri} - x_{Si})\sum_{k=1}^{n}(J_{Rik}U_{kj}) + v_{Ri}U_{ij}\right]}{\displaystyle\sum_{i=1}^{n}\left[(x_{Ri} - x_{Si})\sum_{k=1}^{n}(J_{Rik}v_{Rk}) + v_{Ri}^2\right]}. \tag{18}$$

Finally, according to Eq. (9), the vector $\boldsymbol{d}^0$ is perpendicular to gradf_L, where

$$\operatorname{grad} f_L = \frac{df_L}{d\boldsymbol{x}_L} = \boldsymbol{v}_L + J_L(\boldsymbol{x}_L - \boldsymbol{x}_S), \tag{19}$$

and $J_L = \{\partial v_{Li}/\partial x_{Lj}\}$ is the Jacobian of the vector field $\boldsymbol{v}$ in Eq. (1) evaluated at $\boldsymbol{x}_L$. The steady state $\boldsymbol{x}_S$ is found by solving Eq. (2).

In summary, we have a boundary value problem for an orbit segment, satisfying the boundary conditions (3) and (5) and the steady state condition (2); the unknowns are $\boldsymbol{x}_S, \boldsymbol{x}_L$, and T. There is one more unknown than the equations, therefore one unknown may be taken as a free parameter and this problem is solved by a continuation method [13,14]. The continuation provides a one-parameter family of orbit segments. The separation rate (8) is calculated at each point along this curve according to Eqs. (12)–(19) and searched for maximum and minimum values, indicating the threshold set and the characteristic excitation, respectively. When repeated continuations with sequentially varying external parameters are made, the threshold set and the characteristic excitation can meet and the minimum and maximum values of the separation rate merge and disappear. A second possibility is that the relative amplification r drops below 1 for any of the two extreme orbits thereby violating constraint (11). If either of the two possibilities happen, the excitability vanishes. Since the threshold trajectory is strongly unstable, a multiple shooting method with nonequidistant time subintervals is used in practical calculations [15,16] rather than the simple shooting approach outlined above.

IV. RESULTS AND DISCUSSION

An example of a system providing either oscillatory or excitable dynamics depending on the choice of external parameters is a chemical reaction of bromate with sulfite and ferrocyanide in acidic solution (BSF reaction) run in an isothermal flow-through stirred reactor. This reaction is characterized by large-amplitude oscillations of hydrogen ion concentration and belongs to the group of so called pH oscillators [17]. Dynamics of this system was thoroughly studied experimentally [18] and different mechanisms were proposed [18,19].

Following these studies and our experiments [12,20] we proposed and tested an improved reaction scheme [21,20] which consists of seven irreversible reactions, and four rapidly equilibrated protonation-deprotonation reactions. Based on this mechanism we formulated a 13-variable model that can be further reduced to two variables, and still capture accurately all the experimentally observed dynamics and bifurcation phenomena [20]. On using mass conservation constraints, a charge conservation constraint, a quasi-steady-state and quasiequilibrium assumptions, the model is finally described by two dynamical mass balance equations for hydrogen ions H^+ and hydrogen sulfite ions HSO_3^-. By denoting the molar concentrations $H = [H^+]$ and $HX = [HSO_3^-]$, the equations in a flow-through stirred reactor are formally written as follows:

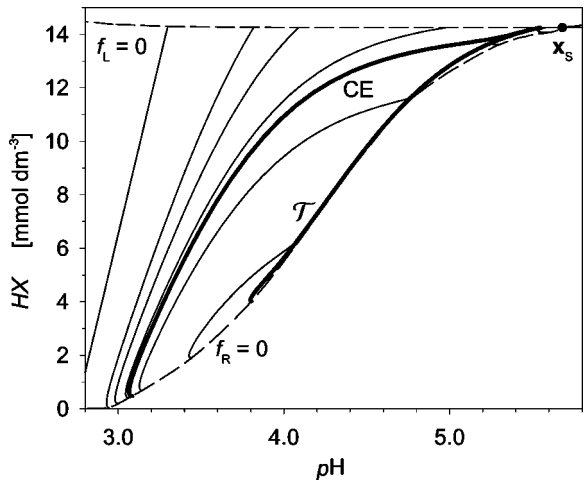

FIG. 2. Phase portrait for the activatory excitability, $k_0 = 4.5 \times 10^{-3}$ s^{-1}, $s_0 = 70$ mM: full lines, orbit segments found by the continuation; the threshold set ($\mathcal{T}$) and the characteristic excitation (CE) are indicated by thick lines; dashed lines show the boundary condition curves, see Eqs. (3) and (5).

$$\frac{dH}{dt} = R_H + k_0(H_0 - H), \tag{20}$$

$$\frac{dHX}{dt} = R_{HX} + k_0(HX_0 - HX). \tag{21}$$

The reaction terms R_H and R_{HX} are rather involved due to the reduction of variables and include contributions to the net reaction rates from both reversible and irreversible steps, see Ref. [20] for details. The external parameters are the flow rate k_0 and the inflow concentrations H_0 and HX_0. However, these two concentrations can be related to the inflow concentrations h_0 and s_0 of the reactants H_2SO_4 and Na_2SO_3 [20]. Consequently, we set $h_0 = 7.5$ mM in correspondence with experiments [20] and take k_0 and s_0 as external control parameters. Fixed concentrations of other reactants are included in R_H and R_{HX}.

For the values $k_0 = 4.5 \times 10^{-3}$ s^{-1} and $s_0 = 70$ mM this model has a weakly acidic steady state SSB (pH≈ 6) and displays excitability upon a perturbation that lowers pH (by adding H^+ ions). Since H^+ ion is the activatory (or autocatalytic) species in the BSF reaction, we call this type of dynamics an *activatory* excitability. The one-parameter family of orbit segments calculated by the continuation method as described in Sec. III is shown in Fig. 2.

Clearly, the threshold set serves as a boundary separating orbits that are excitatory (on the left) and those returning directly to the steady state without any large excursion. Figure 3 shows the dependence of the relative amplification r and the separation rate dr/dP [expressed as $\sinh^{-1}(dr/dP)$ to set proper scale] on the perturbation amplitude P. There is a maximum and a minimum on the dr/dP vs P curve, corresponding to the threshold set and the characteristic excitation, respectively. Figure 3 also shows, that an orbit with maximum amplification is found between the two critical orbits.

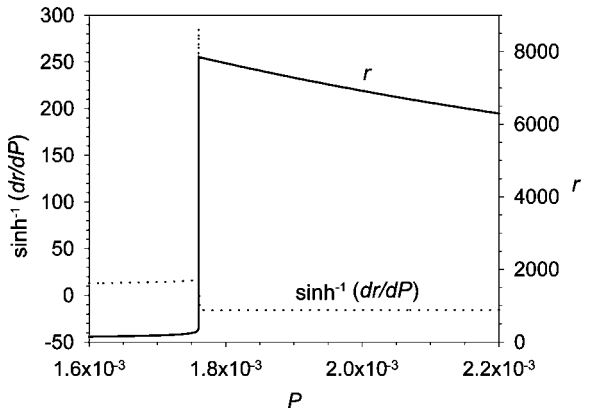

FIG. 3. Dependence of the relative amplification r (full line), and $\sinh^{-1}(dr/dP)$ (dotted line) on the perturbation size P. Parameter values as in Fig. 2.

A complementary case to Fig. 2 occurs at $k_0 = 7.7 \times 10^{-4}$ s^{-1} and $s_0 = 70$ mM, where an acidic steady state SSA (pH≈ 4) exists, see Fig. 4. Here a perturbation that causes excitation should be directed so as to increase pH, for example, by adding OH^- or SO_3^{2-} ions. These species are inhibitors and thus this kind of dynamics is called an *inhibitory* excitability. The calculated dr/dP vs P dependence possesses similar features as that in Fig. 3 and therefore is omitted.

Now we are interested in dependence of both extreme orbits and their characteristics on the flow rate k_0 for fixed values of other parameters. The maximum d_{TS} and minimum d_{CE} of the separation rate dr/dP is plotted against k_0 in Fig. 5. The middle range of k_0 (marked by dashed lines) is the range of stable periodic oscillations. There are two separate maximum/minimum pairs of curves, one extending to the right from the oscillatory range and the other one to the left. Those two separate pairs of branches are associated with the two distinct types of excitability. The right part corresponds to the activatory excitability, see Fig. 2, where excitatory responses at a weakly acidic steady state SSB are invoked by addition of hydrogen ions. The left part is the complementary

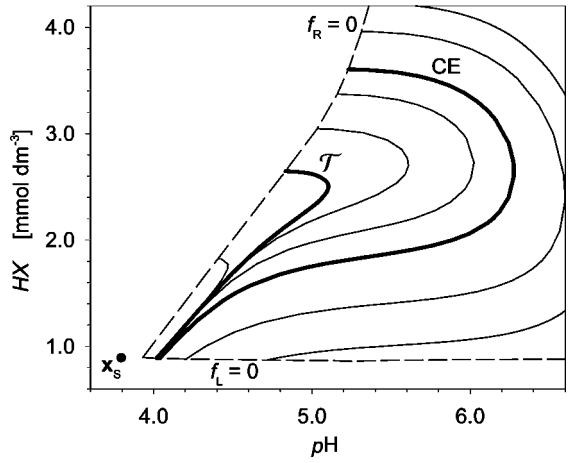

FIG. 4. Phase portrait for the inhibitory excitability, $k_0 = 7.7 \times 10^{-4}$ s^{-1}, $s_0 = 70$ mM; notation of the curves as in Fig. 2.

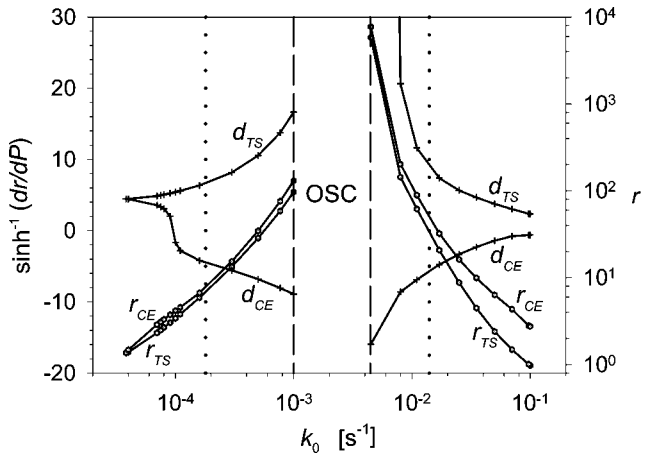

FIG. 5. Dependence of the maximal (d_{TS}) and minimal (d_{CE}) values of $\sinh^{-1}(dr/dP)$ on k_0 at $s_0=70$ mM: dashed lines, bounds of the oscillatory region; dotted lines, bounds of the experimentally observed vanishing excitability.

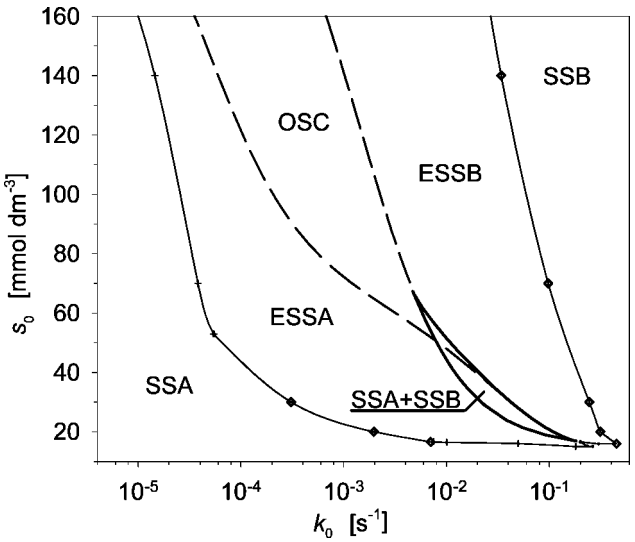

FIG. 6. Bifurcation diagram in the parameter plane k_0-s_0 with marked bounds of vanishing excitability: thin full line, transition from nonexcitable to excitable steady states; thick full line, curve of a saddle-node bifurcation on steady states; dashed line, curve of a Hopf bifurcation.

case of the inhibitory excitability, see Fig. 4, where excitations are elicited by adding hydroxyl or sulfite ions to an acidic steady state SSA; this effectively removes the hydrogen ions.

Along with the values of maxima and minima, we also plot values of the relative amplification for the two extreme trajectories, r_{TS} and r_{CE}. There are two ways of disappearance of excitability depending on whether the constraint (11) holds at the point where Eq. (10) defining the threshold set is violated, or not. Either d_{TS} and d_{CE} merge as k_0 is varied, leaving no extreme trajectories, or condition (11) is violated for an existing threshold set or for its complement, the characteristic excitation. Both cases are found in Fig. 5. On the left side of the oscillatory range the curves d_{TC} and d_{CE} merge at $k_0 \approx 4\times 10^{-5}$ s^{-1} while $r>1$. However, on the right of the oscillatory region r_{TS} drops below 1 at $k_0 \approx 0.1$ s^{-1} well before d_{TS} and d_{CE} merge. For comparison, the dotted vertical lines mark the boundary of vanishing excitability as evaluated from experiments with the BSF system [20]. These experiments rely on measurement of a single species (pH in this case) which can indicate only a strongly developed excitability and that explains a narrower range for excitable dynamics than predicted.

The two limiting values of k_0 for marginal occurrence of excitability depend on other parameters of the BSF system defining thus a boundary of a domain in a parameter space where excitability can be found. By adding s_0 as a second control parameter, we can calculate this boundary as a curve and display it along with other types of curves bounding the domain of excitability, see Fig. 6. The two branches of vanishing excitability meet at a cusp point. A second kind of boundary that delimits the domain of excitability corresponds to two curves where oscillations appear. This is associated either with a supercritical Hopf bifurcation or with a saddle-node bifurcation on periodic orbit which occurs nearby if the Hopf bifurcation is subcritical. Although the latter is the present case, we show only curves of the Hopf bifurcation in Fig. 6 since the saddle-node curves extend very near to the Hopf curves [20]. Finally, the last type of the curve, separating excitability from bistable steady states, is the curve of saddle-node bifurcation on steady states. This curve is closed and includes two cusp points, the lower one coincides with the cusp where two branches of vanishing excitability meet.

Figure 6 shows that the central part, including the oscillatory domain (OSC) and the domain of two coexisting stable steady states (SSA and SSB), separates the two types of excitability. On the left of the central part is the region of inhibitory excitability (ESSA) associated with a perturbation removing hydrogen ions, on the right is the region of activatory excitability (ESSB) associated with a perturbation adding hydrogen ions. Outside the boundaries of vanishing excitability the system is at one of the nonexcitable stable steady states (SSA or SSB). Two parts of the curve of vanishing excitability marked by crosses correspond to the case when the threshold set merges with the characteristic excitation and the relative amplification $r>1$ for both, while the remaining two parts marked by diamonds correspond to $r=1$ for one of the two extreme orbits. Clearly, the vanishing excitability represents a transition that does not change topological structure of the phase portrait, that is, it is not a bifurcation. Rather, it may be compared to a transition from a focal steady state to a node. However, unlike the focus-node transition, the vanishing excitability marks a global change of the phase portrait. A similar dynamical feature (involving also a threshold set) is a sudden amplitude increase of periodic oscillations referred to as canard phenomenon [22,23].

The proposed formulation of the threshold set makes no difference between the two types of excitability. However, it is useful to make this distinction with regard to the way excitability fits into the framework of the *cross-shaped bifurcation diagram* [24] as shown in Fig. 6. The cusp region of multiple steady states and the adjacent oscillatory region is complemented on both sides by the two types of excitability,

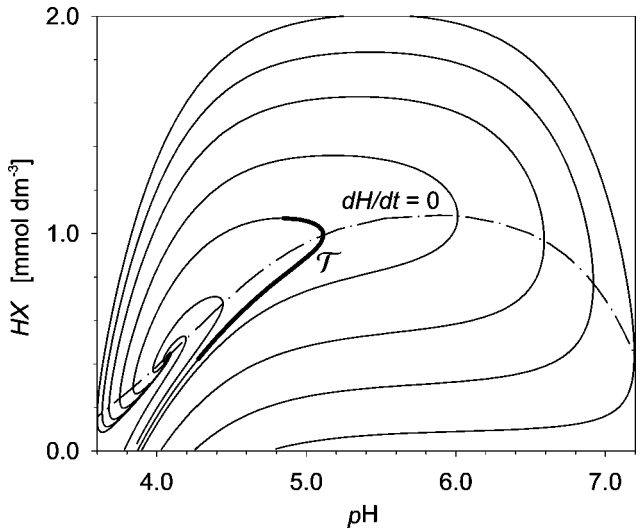

FIG. 7. Phase portrait for the inhibitory excitability showing orbits approaching a focal steady state, $k_0=3\times10^{-4}$ s^{-1}, $s_0=70$ mM; the threshold set $\mathcal{T}$ is indicated by the thick line; the dash-dotted line shows the nullcline for the variable H.

each associated with one of the two stable steady states. The bifurcation structure may be quite symmetric as that in Fig. 6, in which case both types of excitability are well developed, but it may also be asymmetric and then one of the regions of excitability may be small or even absent.

Both the maximum condition (10) and the additional constraint (11) might be altered in a number of ways. We have tried several other formulations and found that all of them provide very similar results in the case of a *strong* excitability, by which we mean cases with a strongly repelling threshold set that passes very close to the steady state. On the other hand, in the case of a *weak* excitability near the point of disappearance, the threshold is usually only weakly repelling and the perturbation amplitude P is relatively large. Under such circumstances only the definition presented here worked well for this and also for a number of other models of excitable systems [21,25].

Among alternative ways of treating excitability threshold there is a commonly accepted approach via nullclines in two-variable systems, see, for example, Refs. [1,4]. The nullclines are obtained by plotting in the phase plane curves of loci where the time derivative for either of the two variables is zero. The intersection(s) of the nullclines defines the steady state(s). For the autocatalytic (fast) variable, there is typically a minimum and a maximum separating the curve into three branches. The middle one repells trajectories and may be taken as the threshold set. Such a situation is found in the FitzHugh—Nagumo-type of equations [1,26,27] where the nullcline for the fast variable is described by a polynomial of third order and the excitable steady state is found on the outer branch past the minimum. In many cases, however, this determination of the threshold is not useful, since the steady state may as well occur on the middle branch and that makes the threshold perturbation impossible to define. This situation is typical for the model represented by Eqs. (20) and (21). For example, at $s_0=70$ mM and $k_0=3\times10^{-4}$ s^{-1}, Fig. 7 compares the nullcline for the autocatalytic variable H and the threshold set satisfying conditions (10) and (11). A similar situation is found by inspecting Figs. 2 and 4. Thus the nullcline method does not allow for determination of the (minimal) threshold perturbation and, in addition, it has the inconvenient feature that the threshold is not invariant with respect to the flow of Eq. (1).

Another way of using the nullcline of the autocatalytic variable to distinguish between subthreshold and superthreshold excursions from an excitable steady state is to take a reference point in the phase plane corresponding to one of the extremes of the nullcline as discussed in Ref. [1]. Trajectories winding around such a point are taken as responses to superthreshold perturbations. Within the context of the threshold set discussed in this paper, the extreme on the nullcline would be the end point of $\mathcal{T}$ associated with a negative semiorbit extending from the extreme. This concept provides results comparable to those for the inhibitory excitability shown in Figs. 4 and 7, where the relevant extreme is the maximum. However, for the activatory excitability shown in Fig. 2 this approach cannot be applied, because the relevant extreme—a minimum—is absent. This turns out to be the rule for the BSF system and is likely to occur in other systems as well. Thus, although intuitive in use, the nullcline approaches have limitations which the current concept of the threshold set avoids. Also, the description of disappearing excitability as parameters are varied is missing with the conventional nullcline methods.

V. CONCLUSIONS

We have outlined a theoretical formulation of a criterion allowing to determine the threshold set—an orbit segment that constitutes a boundary between responses to a perturbation, which are excitatory and those which are not. This formulation leads to a boundary value problem with an added constraint of maximal separation rate. The problem has been solved numerically by employing multiple shooting method for locating an orbit segment satisfying the boundary conditions (3), (5) and the continuation method for finding a segment satisfying the maximum condition (10). The threshold set found in this way can be traced in one or more parameters to find transitions from excitable to nonexcitable dynamics. Such a transition can occur in two different ways: either the threshold set vanishes by merging with a complementary orbit having a minimum value of the separation rate dr/dP or the relative amplification r of either of the two extreme orbits drops below one. Either way, excitable steady states become nonexcitable beyond this transition point. Other transitions include a transition between excitability and oscillations and between excitability and bistable steady states. Although the presented example involves only two variables, extension for systems with three variables is currently being elaborated.

Excitability is usually defined only loosely [28], a quantitative definition such as presented here is helpful when firing sequences in periodically perturbed excitable systems are studied [25,29,30]. In these studies, the knowledge of the threshold set enables us to make a clear distinction between excitatory (superthreshold) and nonexcitatory (subthreshold)

responses and allows for a characterization of the response to periodic perturbations by means of a firing number defined as an average number of excitatory responses per forcing period. Recently there have appeared other approaches to characterizing the threshold in terms of a *T* repeller and isochrones [31,32]. As discussed above, our approach treats both the strong excitability, where the threshold is equivalent to a *T* repeller, and the weak excitability where the concept of strongly repelling sets may be difficult to apply. In addition, the presence of a *T* repeller by itself does not necessarily imply sufficient amplification of the perturbation. The quantitative measure provided by Eq. (10) and the constraint (11) takes into account the distance and position of the threshold set (*T* repeller) from the steady state, which determines sufficient amplification in agreement with intuitive definition of excitability. Moreover, a quantitative measure makes it possible to study transition phenomena associated with the vanishing excitability. The results presented here provide a consistent picture relating excitability to bifurcation phenomena such as subcritical Hopf bifurcation or multiple steady states, a detailed analysis will be subject of our future work.

ACKNOWLEDGMENTS

This work has been supported by grants from the Czech Grant Agency, Grant Nos. 203/02/D051 and 203/03/0488 and a project from the Czech Ministry of Education, Grant No. MSM223400007.

[1] J.D. Murray, *Mathematical Biology* (Springer-Verlag, Berlin, 1989).
[2] D.J. Aidley, *The Physiology of Excitable Cells* (Cambridge University Press, Cambridge, 1998).
[3] J. Rinzel, Bull. Math. Biol. **52**, 5 (1990).
[4] *Some Mathematical Questions in Biology—The Dynamics of Excitable Media*, edited by H. G. Othmer (AMS, Providence, RI, 1988).
[5] J. Keener and J. Sneyd, *Mathematical Physiology* (Springer-Verlag, New York, 1998).
[6] A. Goldbeter, *Biochemical Oscillations and Cellular Rhythms: The Molecular Bases of Periodic and Chaotic Behavior* (Cambridge University Press, Cambridge, 1996).
[7] *Nonlinear Wave Processes in Excitable Media*, edited by A. V. Holden, M. Markus, and H. G. Othmer (Plenum Press, New York, 1991).
[8] R. Kapral and K. Showalter, *Chemical Waves and Patterns* (Kluwer Academic, Dordrecht, 1995).
[9] S.P. Dawson, M.V. D'Angelo, and J.E. Pearson, Phys. Lett. A **265**, 346 (2000).
[10] B. Krauskopf, K. Schneider, J. Sieber, S. Wieczorek, and M. Wolfrum, Opt. Commun. **215**, 367 (2003).
[11] W.D. McCormick, Z. Noszticius, and H.L. Swinney, J. Chem. Phys. **94**, 2159 (1991).
[12] J. Zagora, M. Voslař, L. Schreiberová, and I. Schreiber, Faraday Discuss. **120**, 313 (2001).
[13] M. Kubíček and M. Marek, *Computational Methods in Bifurcation Theory and Dissipative Structures* (Springer-Verlag, New York, 1983).
[14] M. Marek and I. Schreiber, *Chaotic Behavior of Deterministic Dissipative Systems* (Cambridge University Press, Cambridge, 1995).
[15] M. Kubíček and I. Schreiber, Z. Angew. Math. Mech. **77**, S603 (1997).
[16] M. Kohout, I. Schreiber, and M. Kubíček, Comput. Chem. Eng. **26**, 517 (2002).
[17] Y. Luo and I.R. Epstein, J. Am. Chem. Soc. **113**, 1518 (1991).
[18] E. Edblom, Y. Luo, M. Orbán, K. Kustin, and I.R. Epstein, J. Phys. Chem. **93**, 2722 (1989).
[19] G. Rábai, A. Kaminaga, and I. Hanazaki, J. Phys. Chem. **100**, 16 441 (1996).
[20] J. Zagora, M. Voslař, L. Schreiberová, and I. Schreiber, Phys. Chem. Chem. Phys. **4**, 1284 (2002).
[21] M. Voslař, Ph.D. thesis, Prague Institute of Chemical Technology, 2001.
[22] J.L. Callot, F. Diener, and M. Diener, C.R Acad. Sci., Ser. I **23**, 1059 (1978).
[23] M. Brøns and K. Bar-Eli, J. Phys. Chem. **95**, 8706 (1991).
[24] P. De Kepper and A. Pacault, C.R Acad. Sci., Ser. II **286**, 437 (1978).
[25] V. Nevoral, M. Voslař, I. Schreiber, P. Hasal, and M. Marek, FORMA **15**, 199 (2000).
[26] R. FitzHugh, Biophys. J. **1**, 445 (1961).
[27] J.S. Nagumo, S. Arimoto, and S. Yoshizawa, Proc. IRE **50**, 2061 (1962).
[28] J.C. Alexander, E.J. Doedel, and H.G. Othmer, SIAM (Soc. Ind. Appl. Math.) J. Appl. Math. **50**, 1373 (1990).
[29] I. Schreiber, P. Hasal, and M. Marek, Chaos **9**, 43 (1999).
[30] V. Nevoral, V. Votrubová, P. Hasal, L. Schreiberová, and M. Marek, J. Phys. Chem. A **101**, 4954 (1997).
[31] A. Rabinovitch and I. Rogachevskii, Chaos **9**, 880 (1999).
[32] N. Ichinose, K. Aihara, and K. Judd, Int. J. Bifurcation Chaos Appl. Sci. Eng. **8**, 2375 (1998).